Sonochemical dissolution of nanoscale ThO2 and partial conversion into a thorium peroxo sulfate

Laura Bonato, Matthieu Virot, Xavier F Le Goff, Philippe Moisy, Sergey I. Nikitenko

Sonochemical dissolution of nanoscale ThO_2 and partial conversion into a Thorium Peroxo Sulfate

Laura Bonato,[1] Matthieu Virot,[1,*] Xavier Le Goff,[1] Philippe Moisy,[2] Sergey I. Nikitenko[1]

[1] ICSM, Univ Montpellier, CEA, CNRS, ENSCM, Marcoule, France.
[2] CEA, DEN, DMRC, Univ Montpellier, Marcoule, France.
*matthieu.virot@cea.fr

Abstract

The influence of the sample morphology and experimental conditions towards the sonochemical dissolution of nanoscale ThO_2 samples in sulfuric acid media is described. Significant sonochemical dissolution rates and yields are observed at 20 kHz under Ar/O_2 atmosphere in dilute 0.5 M H_2SO_4 at room temperature, contrasting with the generally-reported high refractory behavior for ThO_2. The dissolution of ThO_2 combines the physical effects driven by acoustic cavitation phenomenon, the complexing affinity of Th(IV) in sulfuric medium and the sonochemical generation of H_2O_2. These sonochemical conditions further allow the observation of the partial conversion of ThO_2 into a scarce Th(IV) peroxo sulfate with 1D morphology resulting from one or both following processes: dissolution/reprecipitation or formation of an intermediate Th(IV) surface complex.

1. Introduction

Natural thorium-232 is a weakly radioactive element much more abundant than uranium on earth's crust. Potentially, thorium can be a key to developing a new generation of nuclear fuel for power stations [1,2]. Th-based fuels indeed allow to decrease the production of minor actinides during the burn-up and represent an interesting alternative for the reduction of the proportion of long-lived isotopes (transmutation of minor actinides) [3,4]. Thorium oxide is nevertheless a highly refractory material towards dissolution. The dissolution of ThO_2 in nitric acid solution is very low, particularly because no redox reaction is possible during the dissolution of this oxide [5]. The use of high-fired ThO_2-based fuel thus constitutes a serious problem in the nuclear fuel cycle in particular for the reprocessing step [6]. Several studies have reported that the addition of small amounts of hydrofluoric acid as surface complexing agent in nitric aqueous solutions dramatically enhances the dissolution of thorium oxide [7–10]. Simonnet et al. proposed recently a dissolution mechanism for ThO_2 in HNO_3-HF mixture which takes into account the important effect of HF and the related formation of ThF_4 [11]. Other processing methods have been reported by changing the dissolution medium with CF_3SO_3H [12] or H_3PO_4 [13] for instance, or by using alternative techniques such as pyrochemistry [14], autoclaves and microwaves [13,15]. Nevertheless, these methods are difficult to be applied in the current reprocessing processes because of safety requirements and due to the high corrosion of the equipment with fluoride ions.

Nanosized thorium oxide may be suggested as a more reactive thorium-based fuel. Nanostructured materials can be defined as materials with a substructure of the order of a few nanometers (1-10 nm) [16,17]. These materials are of growing interest due to their attractive physical and chemical properties potentially optimized through their size,

morphology and structure [18,19]. The nanoscale particles or crystallites composing these materials have a large surface-to-volume ratio and provide a greater amount of active sites in comparison to bulk materials thus increasing their reactivity. In parallel, ThO_2 is largely studied because of its isomorphism with other tetravalent actinide oxides, its low solubility in aqueous solutions and its good resistance to irradiation [20–22]. Particularly, Th(IV) crystallizes as oxide in the CaF_2 fluorite crystal system (Fm-3m space group) similarly with UO_2 and PuO_2. Furthermore, nanoscale actinide oxides are currently stirring up the curiosity of scientists due to their potential contribution in environmental migration of actinides and the safety considerations related to interactions with groundwater during storage of spent nuclear fuel. Thorium, which only exists at the +IV oxidation state, therefore, offers the possibility of simulating the behavior of Pu-based oxide materials in less restrictive conditions without any contribution of redox processes (with however a difference in ionic radii for both elements: 1.05 Å against 0.96 Å for Th(IV) and Pu(IV), respectively, in 8-fold coordination [23]).

Sonochemistry appears as a suitable alternative for the dissolution of refractory materials and its efficiency towards dissolution has been reported with various refractory materials, including oxides such as ThO_2, PuO_2, CeO_2, etc. [24–26] The influence of sonication and HNO_3 concentration has, for instance, been discussed during the dissolution of uranium carbide in nitric aqueous solutions [27]. In addition to the well-known physical effects driven by the acoustic cavitation, which generally dramatically enhance solid materials reactivity (e.g., surface erosion, particle fragmentation, mass transfer, etc.), the sonochemical in-situ generation of active species (H_2O_2, HO°, HO_2°, H_2, Ti^{3+}, etc.) has been reported to significantly improve the dissolution of PuO_2 and CeO_2 in aqueous nitric acid solutions [28,29]. More recently, a study highlighted the accumulation of intrinsic Pu(IV) colloids during the 20 kHz sonolysis of PuO_2 in pure water under Ar/(10%)CO atmosphere [30]. Moreover, it has been reported that sonochemistry can also induce the phase conversion of a solid. The topotactic conversion of chloroapatite into hydroxyapatite was for instance achieved by sonication of the former in deionized water (25°C) at 35 kHz [31]. In another study, the transformation of anatase into rutile was observed during the synthesis of nanostructured TiO_2 via ultrasound assisted sol-gel technique [32]. This paper focuses on the sonochemical behavior of nanoscale ThO_2 powders in pure water and dilute aqueous solutions of H_2SO_4. H_2SO_4 has been selected because of its stability under ultrasound irradiation in combination to previous reports that demonstrated its significant effect towards dissolution when compared to other conventional inorganic acids [33]. The reactivity of these materials is compared in terms of sonochemical effect towards dissolution and morphology evolutions. Particularly, the significant dissolution of ThO_2 and its partial conversion into a scarce Th peroxo sulfate is reported.

2. Experimental Section

Caution! *^{232}Th is an α-emitting radioisotope and standard precautions should be followed for handling this chemical element.*

2.1. Syntheses

All the used reagents were of analytical grade and were supplied by Sigma-Aldrich. The various aqueous solutions were prepared using deionized water (18.2 mΩ.cm at 25°C). Nanostructured thorium oxide samples exhibiting platelet morphology (n-STR) were

obtained by the conventional oxalic route [4,29,34]. Briefly, a 0.1 M thorium solution was prepared at room temperature by dissolving 3.239 g of $Th(NO_3)_4.5H_2O$ in 50 mL of 1 M nitric acid solution before being slowly added to 53.89 mL of 0.5 M oxalic acid solution (previously prepared by dissolving 6.3 g of oxalic acid in 100 mL of 1 M nitric acid). One hour after mixing the solutions (using a magnetic stir bar), Th(IV) oxalate precipitate was separated from the supernatant by centrifugation (9000 rpm during 5 min), washed twice with water and dried at room temperature under vacuum. The reference material (ThO_2 bulk) was obtained by firing Th(IV) oxalate precipitates (similar to nanostructured ThO_2) in air at 1000 °C during 2 h.

Thorium oxide nanopowders (n-PWD) were obtained in basic conditions in the presence of a polymer at room temperature [35]. A 0.1 M thorium solution was prepared by dissolving 3.239 g of $Th(NO_3)_4.5H_2O$ with 0.033 g of polyethylene glycol (PEG, M= 3000 $g.mol^{-1}$, 2.5 wt.%) in 50 mL of water. A solution of NH_4OH (30%) was slowly added to the thorium solution until the pH reached a value of 10 (about 3 mL). One hour after mixing the solutions (using a magnetic stir bar), Th(IV) hydroxide precipitate was separated from the supernatant by centrifugation (9000 rpm during 5 min), washed twice with water and dried at room temperature under vacuum. The different precursors (oxalate and ammonia routes) were then calcined under air at 485°C (during 2 h or 4 h) to obtain ThO_2 exhibiting different refractory behavior according to their nanoscale morphology (nanostructured, n-STR vs. nanopowder, n-PWD) and particle size (crystallites) differences [36].

Table 1 summarizes the SEM, HR-TEM and S_{BET} characterizations performed on the ThO_2 samples. The nanostructuration (n-STR) of the oxides prepared by thermal conversion of oxalate precursors at 485°C is evidenced by HR-TEM with the observation of sintered nanoparticles (or crystallites) forming squared platelets. These nanoparticles are found to be monodispersed, quasi-spherical and crystalline, and measure about 7.6 ± 2.1 nm in diameter. Thorium oxide nanopowder (n-PWD), synthesized at 485°C from basic conditions, is also composed of agglomerates of spherical, monodispersed and crystalline nanoparticles measuring about 7.7 ± 1.4 nm. These values contrast with the high sizes of the coherent domains already reported for ThO_2 calcined at high temperature (fired at 1000°C and used as a reference material in this study) but agree with a previous report evidencing the small crystallite sizes for low fired oxide precursors [36]. HR-TEM measurement of nanoparticle size are found to be consistent with values obtained from XRD (**Table 1**, Rietveld refinement) thus confirming our observations and extracted values.

Table 1: ThO_2 sample characteristics and related nanoparticle sizes composing them and the sonolysis residues in different media (20 kHz, Ar/(20%)O_2, 20°C, 0.34 $W.mL^{-1}$) both determined by HR-TEM and XRD measurements (Rietveld refinement, when possible).

	Nanostructured ThO_2 (n-STR)		**ThO_2 nanopowder (n-PWD)**		**Reference material ThO_2**	
Synthesis route (conditions)	oxalic route (485°C, 4 h)		basic route (485°C, 2 h)		oxalic route (1000°C, 2 h)	
SEM morphology	Squared platelets		Agglomerated NPs		Squared platelets	
S_{BET} ($m^2.g^{-1}$)	13.5 ± 0.1		82.4 ± 0.1*		4.7 ± 0.1	
Particle size (nm)	*HR-TEM*	*XRD*	*HR-TEM*	*XRD*	*HR-TEM*	*XRD*
	7.6 ± 2.1	6.4 ± 0.7	7.7 ± 1.4	5.7 ± 0.1	66.6 ± 27.1	63.6 ± 1.5
Particle size for the sonolysis residue (nm)						

Water	8.8 ± 2.2	9.1 ± 0.9	7.0 ± 1.7	7.5 ± 1.1	-
0.05 M H_2SO_4	7.6 ± 1.5	-	6.2 ± 1.2	-	-
0.5 M H_2SO_4	7.9 ± 1.2	-	-	-	-

*value taken as an indicator from a previous report (ThO_2 n-PWD prepared at 450°C)[35]

2.2. Sonochemical experiments

Two kinds of sonochemical reactors were used in this study, depending on the applied frequency. The experiments at low frequency ultrasound (20 kHz) were performed in a thermostated batch reactor containing 50 mL of solution with controlled saturating gas. Ultrasound was supplied with a 1 cm^2 titanium alloy probe fitted on top of the reactor and connected to a 750 W generator (Sonics & materials, Vibracell VCX 750) [37]. The experiments at high frequency ultrasound (345 kHz) were performed in a thermostated cylindrical reactor (250 mL of solution) mounted on top of a 25 cm^2 high-frequency transducer (ELAC Nautik) and connected to a 125 W multifrequency generator. For high frequency experiments, an additional mechanical stirring fixed at 100 rpm was ensured by a glass blade to homogenize the suspensions and avoid formation of standing waves. For all of the experiments, the solution was sparged with Ar/(20%)O_2 about 20 min before sonication and during the whole ultrasonic treatment at a controlled rate of 100 $mL.min^{-1}$. Some of the experiments have been performed in the presence of Ar/(10%)CO gas mixture. Carbon monoxide is known to be an effective scavenger of OH radicals leading to the inhibiting of H_2O_2 formation [38]. The temperature inside the reactor during the sonolysis was maintained at 20°C with a cryostat (Lauda Eco RE 1050) connected to the reactors. The temperature was measured by a thermocouple immersed into the solution. The acoustic power density, P_{ac} ($W.mL^{-1}$), transmitted to the solution, was measured using the conventional thermal probe method [37] and reached 0.34 and 0.19 $W.mL^{-1}$ at 20 and 345 kHz, respectively. All the experiments were performed with the same quantity of thorium oxide powders (3.5 $g.L^{-1}$) that was suspended in different aqueous solutions (H_2O, 0.05 M H_2SO_4, 0.5 M H_2SO_4). The sonolyses of the different solutions without any powder were considered as reference experiments.

2.3. Analyses and characterizations

UV-Vis absorption spectroscopy. The sonochemical formation of H_2O_2 was followed by UV-Vis absorption spectroscopy. During sonolysis, aliquots of solutions (1 mL) were collected with a syringe through a septum and filtered with 0.2 µm PTFE filters (without any volume adjustment). Then, a small volume of the as-collected solution was mixed (1:1) with a 0.02 M Ti(IV) solution (previously prepared in 0.5 M H_2SO_4 by dissolution of $TiOSO_4$ salt) to form a yellow complex absorbing at 410 nm (ε= 722 $cm^{-1}.M^{-1}$). A calibration curve was previously plotted with a commercial H_2O_2 solution previously titrated with a $KMnO_4$ solution. Absorption spectra were recorded in a 1 cm quartz cell from 280 to 800 nm using a Thermo Evolution 220 spectrophotometer. The statistical error for H_2O_2 formation rate was estimated to be lower than 10%.

Inductively Coupled Plasma - Optical Emission Spectroscopy (ICP-OES). The sonochemical dissolution of ThO_2 was followed by ICP-OES analysis with a Spectro Arcos apparatus (Spectro Analytical Instruments GmbH) equipped for axial plasma observation. A small volume of the collected solution aliquots (described above) was diluted with 0.3 M HNO_3 in the appropriate range of concentration prior to analysis. The concentration of thorium in solution was determined against an external calibration curve (0.1-15 $mg.L^{-1}$) prepared with

certified standard solutions of 1000 µg.mL^{-1} (SCP Science). The thorium content in solution was followed using several analytical wavelengths (401.913, 283.730, 274.716, 283.231 nm). The given value is a mean of three replicates. The statistical error for ThO_2 dissolution rate was estimated to be lower than 10%.

S_{BET} measurements. The specific surface area of ThO_2 samples (Table 1) was determined using nitrogen adsorption at 77 K after overnight degassing under vacuum at 573 K with a Micromeritics ASAP 2020 apparatus.

Powder X-Ray Diffraction (PXRD). PXRD diagrams were obtained with the use of a Bruker D8 Advance X-ray diffractometer equipped with a linear Lynx-eye detector (Cu $K\alpha_{1,2}$ radiation, λ = 1.54184 Å). PXRD patterns were recorded between 5° and 120° (θ-2θ mode) at room temperature, with a step size of Δ(2θ) = 0.02° and a counting time of 1.8 s.step^{-1}. Powder X-Ray Diffraction (PXRD) confirmed the characteristic patterns of the fluorite structure (Fm-3m space group) typical for ThO_2 for all of the studied samples in agreement with the literature and our previous report [36]. LaB_6 measurements were used to extract the instrumental functions. The collected data were refined by the Rietveld method when possible using the Fullprof_suite package [39].

Raman spectroscopy. Raman spectra were collected using a Horiba – Jobin Yvon Aramis apparatus equipped with an edge filter and a Nd:YAG laser (λ = 532 nm). The laser beam was focused onto the sample simply deposited on a glass lamella (1 µm^2) with the use of an Olympus BX41 microscope. The spectra were recorded between 100 and 1500 cm^{-1}. Before the analysis of the sample, the apparatus was calibrated with a silicon wafer, using the first-order Si line at 520.7 cm^{-1}.

Scanning Electron Microscopy (SEM). The starting oxides and the solid residues obtained after sonolysis were characterized with SEM using a FEI Quanta 200 electron microscope. The samples were directly deposited onto carbon tapes without additional preparation.

High-Resolution Transmission Electron Microscopy (HR-TEM). HR-TEM measurements were performed with a Jeol 2200 FS microscope (200 kV) equipped with a CCD GATAN USC camera. For HR-TEM analyses, sample aliquots were dispersed in absolute ethanol or pure water using an ultrasonic bath. One drop was then deposited onto a carbon-coated copper grid which was air-dried prior to analysis. For chemical analysis, the samples were characterized by Energy-Dispersive X-ray Spectroscopy (EDS) using a Silicon Drift Detector (SDD). Particle size measurements from HR-TEM analyses were determined by a statistical measurement using Image J software. The average value was given from at least 50 parallel measurements.

3. Results and Discussion

3.1. Effect of the different media on ThO_2 dissolution

The sonication of nanoscale ThO_2 powders (nanostructured ThO_2, n-STR, from oxalic route and ThO_2 nanopowder, n-PWD, from basic route) in aqueous solutions allows the observation of Th(IV) accumulation in solution as well as the formation of a solid residue at the end of the experiment (obtained by centrifugation and water washing of the sonicated mixture). Th(IV) accumulation kinetics are compared in **Figure 1** for the different aqueous

systems. A comparable behavior can be noticed for both sonicated ThO_2 samples which are found highly resistant in pure water but significantly dissolve in sulfuric media. The dissolution rates and yields are furthermore found to significantly increase from 0.05 M H_2SO_4 to 0.5 M H_2SO_4 for ThO_2 n-STR. Higher yields (38% dissolved in 0.5 M H_2SO_4 in 900 min) are nevertheless observed for ThO_2 n-PWD which in addition exhibits practically zero-order dissolution kinetics. The complexing affinity of sulfate-anion with Th(IV) cation has been reported to enhance the dissolution of ThO_2 with the formation of surface complexes at the solid/liquid interface [33]. The dissolution kinetics differences for both oxides can be related to their morphology and specific surface area. ThO_2 n-STR is indeed composed of square platelets assembled from sintered particles whereas ThO_2 n-PWD is composed of small grain aggregates which facilitate its dissolution (increased surface availability). The induction period observed for the nanostructured sample (ThO_2 n-STR) at the beginning of its dissolution can be attributed to a first induction period related to platelets breaking and fragmentation which increase the available surface area and reactivity of the powder and improve the dissolution rate of the oxide.

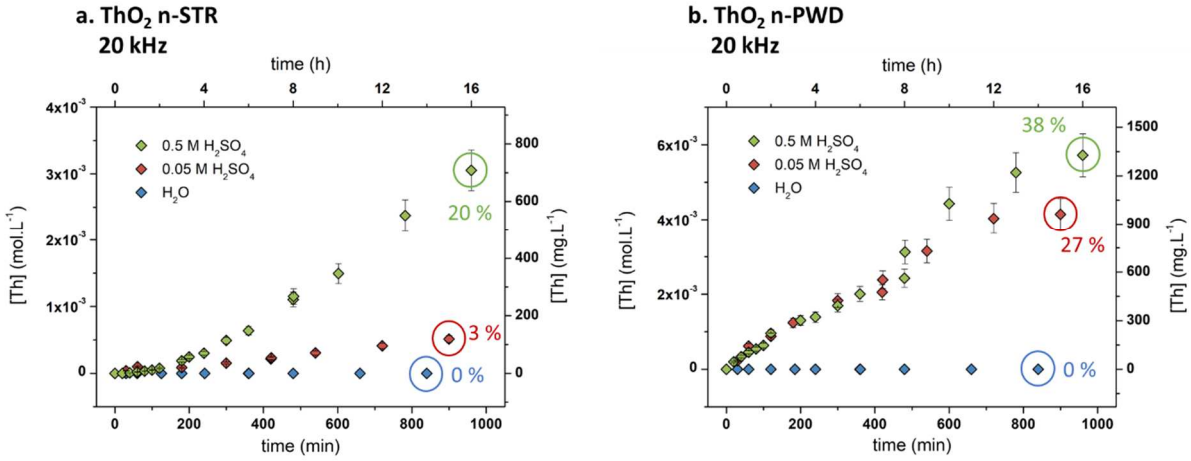

Figure 1: ThO_2 dissolution curves observed under 20 kHz ultrasound (20°C, Ar/(20%)O_2, 0.34 W.mL^{-1}) in pure H_2O, 0.05 M H_2SO_4 and 0.5 M H_2SO_4 for (a.) ThO_2 n-STR and (b.) ThO_2 n-PWD.

3.2. Sonication effect on ThO_2 dissolution

The effect of the ultrasonic wave and applied frequency on the dissolution rate of nanostructured ThO_2 and ThO_2 nanopowder in 0.05 M H_2SO_4 is illustrated on **Figure 2**. Whatever the oxide, mechanical agitation without ultrasound (silent conditions) does not lead to significant accumulation of Th after 480 minutes of treatment. **Figure 2** also demonstrates the significant effect of low frequency ultrasound for the dissolution of these refractory ThO_2 samples which usually requires the addition of fluoride ions in concentrated nitric acid medium [10]. A lower dissolution rate is indeed observed when applying high frequency ultrasound (345 kHz) in comparison to low frequency experiment (20 kHz). Generally, chemical effects have been reported to be favored at high frequency whereas 20 kHz ultrasound generates stronger physical effects expressed by surface erosion, particle fragmentations, decrease of diffusion layers, etc. As described above (see part 3.1.), this effect is clearly observable when comparing the sonochemical initial dissolution rates of nanostructured ThO_2 and ThO_2 nanopowder on **Figure 1**. Whereas Th accumulation rates is found linear when considering ThO_2 nanopowder, the ultrasound-assisted dissolution of nanostructured ThO_2 indeed shows a time-increasing accumulation rate for Th (not linear)

evidencing an induction period at the first stage of dissolution. Such observation also explains that for similar conditions, higher yields are observed with n-PWD samples in comparison to n-STR (**Figure 2.a.** vs. **2.b.**).

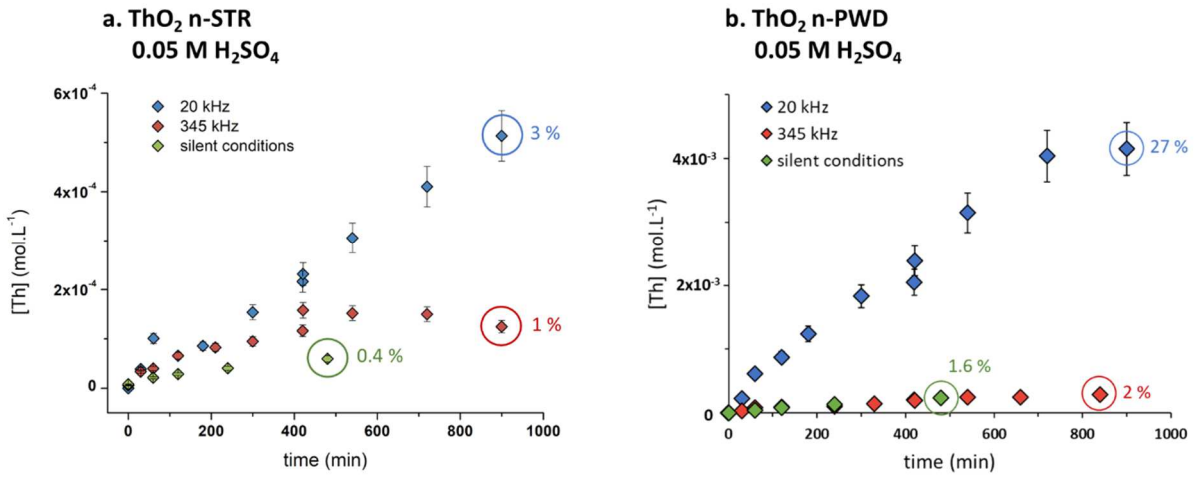

Figure 2: Dissolution curves (Ar/(20%)O_2, 20°C) observed for (a.) ThO_2 n-STR and (b.) ThO_2 n-PWD suspended in 0.05 M H_2SO_4 at 20 kHz (0.34 W.mL^{-1}), 345 kHz (0.19 W.mL^{-1}) and in silent conditions.

3.3. Effect of the H_2O_2 formation on ThO_2 dissolution

The sonication of these samples in aqueous solutions (pure H_2O, 0.05 M H_2SO_4 and 0.5 M H_2SO_4) allowed to observe the accumulation of H_2O_2 which initial kinetics ($W_0(H_2O_2)$), measured in the presence or absence of ThO_2 powder, are represented in **Figure 3**. The kinetic values related to the initial H_2O_2 formation rates are gathered in **Table S1, ESI**. The higher formation rates observed at high frequency ultrasound (345 kHz) compared to low frequency at 0.05 M H_2SO_4 are attributed to the dissociation of O_2 molecules in the cavitation bubble and the recombination of the generated radical products which increase H_2O_2 accumulation rates through various mechanisms [40–43]. In the studied experimental domain, the initial H_2O_2 formation rate shows a decreasing trend in the presence of ThO_2 powder whatever the medium or the applied acoustic frequency except for the experiment carried out in 0.5 M H_2SO_4. Several hypotheses may explain the general tendency for H_2O_2 kinetics observed in the presence of oxide, including: (i) the complexation or catalytic decomposition of H_2O_2 on the surface of the oxide [35], (ii) the complexation reaction between H_2O_2 and dissolved Th(IV) [44–46], (iii) the redox or complexation reactions of H_2O_2 with Ti products resulting from the sonotrode erosion (only at 20 kHz), which is significantly depassivated in sonicated sulfuric media. Probably, the discrepancies noted in 0.5 M H_2SO_4 regarding H_2O_2 accumulation rates can be partly attributed to interactions with Ti products. Note that a previous work reported a similar decrease in H_2O_2 formation rate in the presence of oxide powder related to a catalytic H_2O_2 decomposition [35]. Further work must be performed to explain the differences observed in the initial H_2O_2 formation in sulfuric acid media.

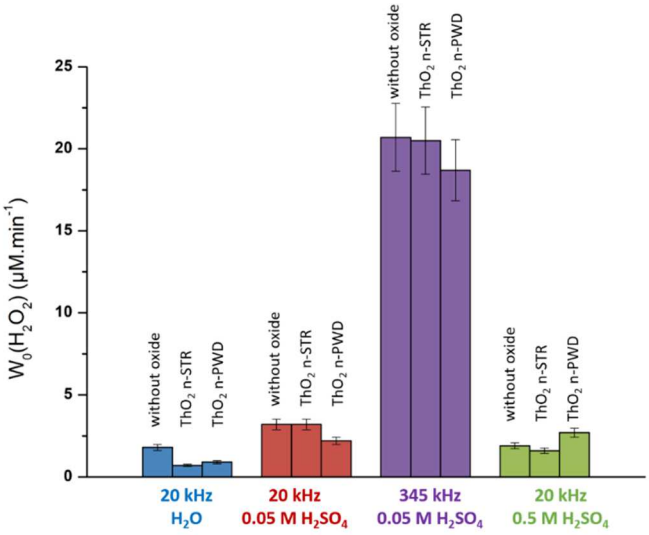

Figure 3: Representation of the initial H_2O_2 formation rates observed in the different sonicated media (Ar/(20%)O_2, 20°C) for ThO_2 n-STR and ThO_2 n-PWD calcined at 485°C at 20 kHz (0.34 W.mL^{-1}) or 345 kHz (0.19 W.mL^{-1}).

The effects of the saturating atmosphere (Ar/20%O_2, Ar/10%CO, Ar) and the addition of H_2O_2 on the sonochemical dissolution rate of ThO_2 n-STR at 20 kHz are illustrated in **Figure 4**. In 0.5 M H_2SO_4, the ultrasound-assisted dissolution rate of ThO_2 n-STR is much lower under Ar and Ar/CO than under Ar/O_2. In the presence of O_2, the formation rate of H_2O_2 is enhanced because of the scavenging of H radicals by O_2 [42,43]. Conversely, the presence of CO, which reduces the dissolution rate, inhibits the accumulation of H_2O_2 similar to that observed in homogeneous aqueous solutions. In addition to the importance of the physical effects reported in part 3.2., these results confirm that the sonochemical generation of H_2O_2 significantly affect the dissolution of thorium oxide (**Figure 1**). This last assertion is confirmed with the observation of a significant increase of Th accumulation rate when adding hydrogen peroxide ([H_2O_2] = 0.01 M) in the reactor during the 20 kHz sonication of nanostructured ThO_2 in 0.05 M H_2SO_4 (**Figure 4.b.**). It is interesting to note that these observations agree with previous investigations that demonstrated the significant effect of dilute hydrogen peroxide solutions for ThO_2 dissolution in comparison to conventional inorganic acids (in silent conditions).[33]

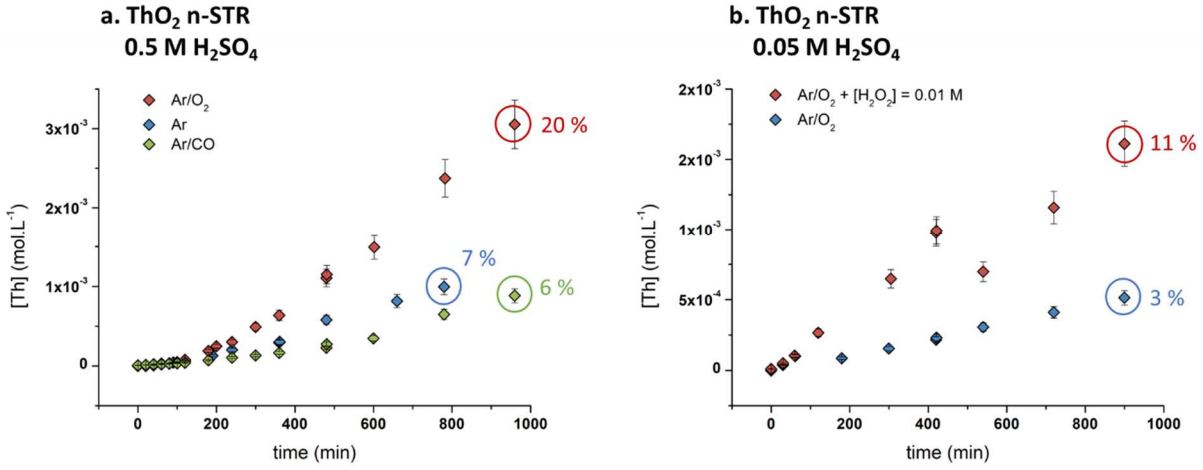

Figure 4: (a.) Sonochemical dissolution curves observed for nanostructured ThO_2 in 0.5 M H_2SO_4 at 20 kHz (20°C, 0.34 $W.mL^{-1}$) for the different atmosphere used. (b.) Sonochemical (20 kHz, Ar/(20%)O_2, 20°C, 0.34 $W.mL^{-1}$) dissolution curves for nanostructured ThO_2 suspended in 0.05 M H_2SO_4 without the addition of H_2O_2 and in the presence of 0.01 M H_2O_2 introduced in the reactor at t = 0 min.

3.4. Characterization of the residual solid phase

SEM images acquired on the dissolution residues (obtained by centrifugation and pure water washing of the suspension mixture during sonolysis) generated in water during the treatment of the nanostructured sample (ThO_2 n-STR, oxalic route) confirm the progressive size reduction of the oxide platelets in agreement with the sonication time (**Figure 5**). This phenomenon is attributed to the physical effects driven by the collapsing acoustic bubbles (micro-jets, shock waves, particle collisions, etc.). The contrasting higher refractory behavior of reference ThO_2 calcined at 1000°C has been confirmed by studying its sonochemical reactivity in 0.5 M H_2SO_4 (**Figure S1, ESI**). For a similar platelet morphology, the resulting dissolution rate is much lower than that observed for the nanoscale oxide calcined at 485 °C which agree with the generally-observed increased refractory behavior of high-fired oxides. This can be related to its lower specific surface area (**Table 1**) which results from the elimination of the porosity and crystal defects that occur when increasing the firing temperature or duration. Several studies already evidenced the relation between the specific surface area of the oxide and its dissolution in acidic solutions [21,47]. Furthermore, a nanoscale effect often linked to the improved number of surface active sites, lattice stress, strains, etc. can also be proposed for the oxides fired at 485°C. It is important to remind that ThO_2 is known to be highly refractive towards dissolution, the here observed significant dissolution can be related to the nanoscale composition of the oxides made out of ca. 7 nm nanoparticles. Previous studies already demonstrated that nanomaterials may offer significantly improved reactivity or physico-chemical properties [17,19,30,48]. Despite these important effects, the absence of dissolution for ThO_2 powders in pure H_2O as reported in **Figure 1** (see part 3.1.), and inhibiting effect of CO (see **Figure 4.a.** in part 3.3.) indicate that the dissolution mechanism of ThO_2 does not result solely from the physical effects of ultrasound but also depends on other parameters such as the complexing nature of the medium.

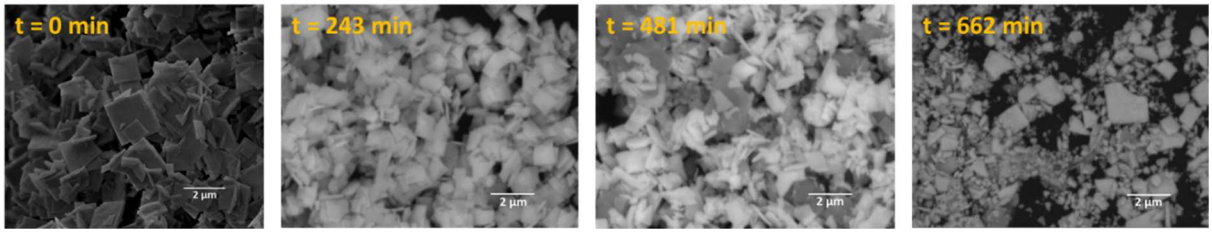

Figure 5: SEM images acquired on the starting nanostructured ThO_2 (485°C) and its corresponding sonolysis residue obtained in pure H_2O for different sonolysis times (20 kHz, Ar/(20%)O_2, 20°C, 0.34 $W.mL^{-1}$).

The effects of the acoustic cavitation on both nanoscale oxides sonicated in sulfuric acid medium are showed on the HR-TEM pictures obtained on the corresponding dissolution residues (**Figure 6)**. Sonication of these oxides in dilute sulfuric acid solution leads to the strong platelets size reduction and fragmentation without significant modification of the crystallite size (see **Table 1**).

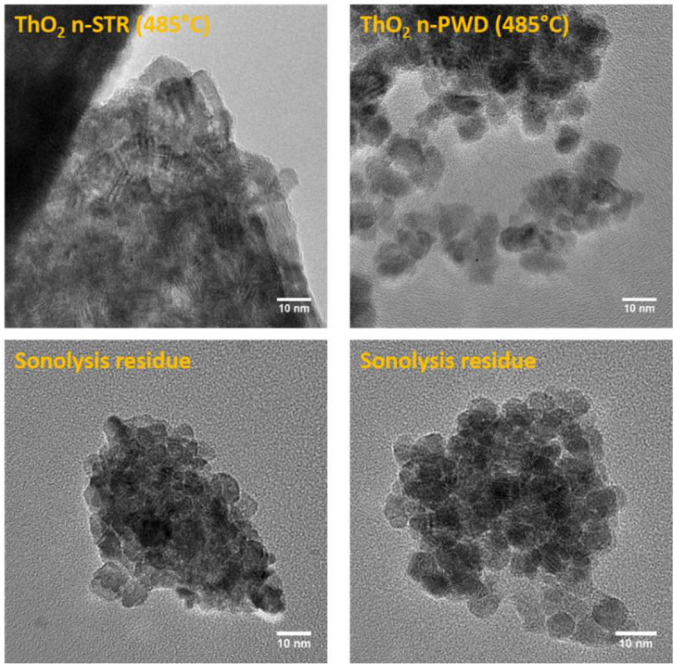

Figure 6: HR-TEM images of the starting nanostructured or nanopowdered ThO_2 samples and their corresponding sonolysis residues observed in 0.05 M H_2SO_4 (20 kHz, Ar/(20%)O_2, 20°C, 0.34 W.mL^{-1}).

Raman spectra of the starting ThO_2 samples and corresponding sonolysis residues obtained in sulfuric medium are gathered in **Figure 7** and **Figure S2 (ESI)**. Both starting ThO_2 samples spectra are also compared to the one of the reference material ThO_2 calcined at 1000°C. An enlargement of the T_{2g} band located at 465 cm^{-1} (FWHM) is observed with the decrease of the calcination temperature of ThO_2 samples. This phenomenon is a fingerprint for nanocrystals and can be explained by the confinement of optical phonons in nanosized particles (crystallites) in agreement with the literature [49–53]. Further enlargement of the FWHM combined to a red shift of the T_{2g} band is clearly observed for the sonicated nanoscale ThO_2 sample residues. A similar observation has been made on nanostructured sample residues (ThO_2 n-STR) after sonication in pure water (**Figure S3, ESI**) evidencing that the observed peak features are not related to the dissolution progress itself. The enlargement of the FWHM parameter is generally attributed to the shrinking particle size of oxide nanocrystals while the red shift is often correlated with the presence of defects, volume expansion, grain size distribution, etc. [49] The evolution of these two parameters for the T_{2g} band of the sonolysis residues cannot be explained by a particle size reduction since the size of the nanoparticles composing ThO_2 powders are found similar before and after sonication (**Table 1 and Figure 6**).

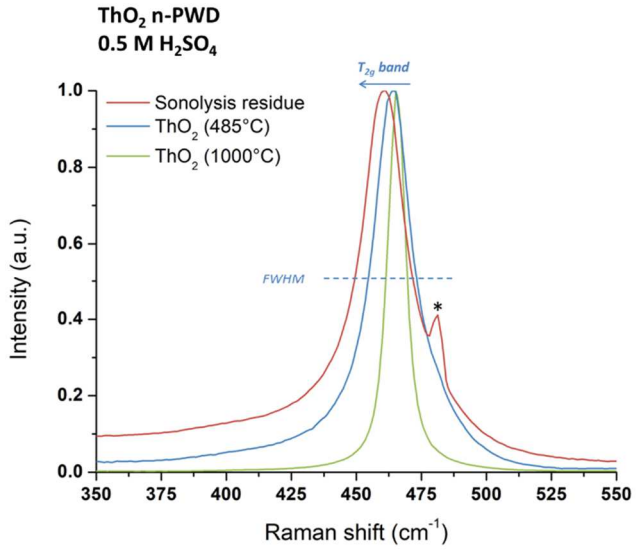

Figure 7: Normalized Raman spectra observed on reference material ThO_2 (1000°C), nanopowdered (n-PWD) ThO_2 (485°C) and its sonolysis residue obtained in 0.5 M H_2SO_4 (20 kHz, Ar/(20%)O_2, 20°C, 0.34 W.mL^{-1}). *artefact attributed to dust on the mirror of the spectrometer.

By contrast, the increased generation of strains, defects, and stress provided by the acoustic cavitation at the surface of the nanoparticles could significantly favor the interface reactivity involving a shift and enlargement of the T_{2g} band. Such effects influence the atomic surface configuration and its potential hydration and hydrolysis can be viewed as an additional surface stress that may influence these two processes. Particularly, surface hydrolysis kinetics has been reported to exhibit significant geometry variation (in comparison to ThO_2) and strongly depend on the concentration and nature of surface defects [54,55]. In addition, the catalytic activity of many metal centers is known to be partly determined by the strength and amount of Lewis and Brønsted acid-base sites standing at the surface of the catalysts. ThO_2 exhibit catalytic properties (which are strengthened at the nanoscale) and ultrasonic treatment may increase the surface concentration of such moieties.

3.5. Partial conversion of ThO_2 into a thorium peroxo sulfate

The sonolysis residues recovered after treatment of the nanoscale ThO_2 powders in different aqueous solutions were characterized by PXRD analysis (**Figure 8** and **Figure S4, ESI)**. The PXRD diagrams for the starting ThO_2 samples are gathered on **Figure S5, ESI**. The sonication residue diagrams for the nanoscale oxides display the characteristic patterns of the fluorite structure (Fm-3m space group) typical for ThO_2 (ICSD 01-071-6407). Some diffraction peaks corresponding to Ti (ICSD 00-044-1294) and attributed to the sonotrode erosion during the prolonged 20 kHz ultrasonic treatment, can also be observed. The PXRD diagrams of the sonolysis residues obtained in sulfuric acid (0.05 M and 0.5 M) also show some additional diffraction peaks principally located at small angles that are not observed for the sonolysis residue obtained in pure water. These PXRD patterns correspond to a recently studied thorium peroxo sulfate, $Th(O_2)(SO_4)(H_2O)_2$, which crystallizes in the space group $Pna2_1$ of the orthorhombic system as evidenced by a combination of synchrotron PXRD and EXAFS approaches [56]. In this compound, peroxo ligands coordinate Th centers in a scarce μ_3-η^2:η^2:η^2 bridging mode forming infinite 1D chains decorated with sulfato ligands. The corresponding purple PXRD diagram presented in **Figure 8** shows diffraction peaks matching with those observed at small angles for the sonolysis residues. This result indicates the partial conversion of both nanoscale ThO_2 samples into a thorium peroxo sulfate during

sonolysis. The low intensity of the diffraction peaks for this neoformed compound indicates its low proportion in the sample residue as well as its low crystallinity. This observation combined with the atomic form factor explains that the diffraction peaks at 2θ> 20° are poorly distinguishable. Furthermore, the crystallinity of the Th peroxo sulfate in silent conditions has been demonstrated to strongly depend upon the synthesis medium as evidenced in **Figure S6 (ESI)** which strengthens the observed low intensity of the diffraction peaks in the residue but also explains the better crystallinity noticed on XRD diagrams for this new compound in 0.05 M H_2SO_4 (in comparison to 0.5 M H_2SO_4).

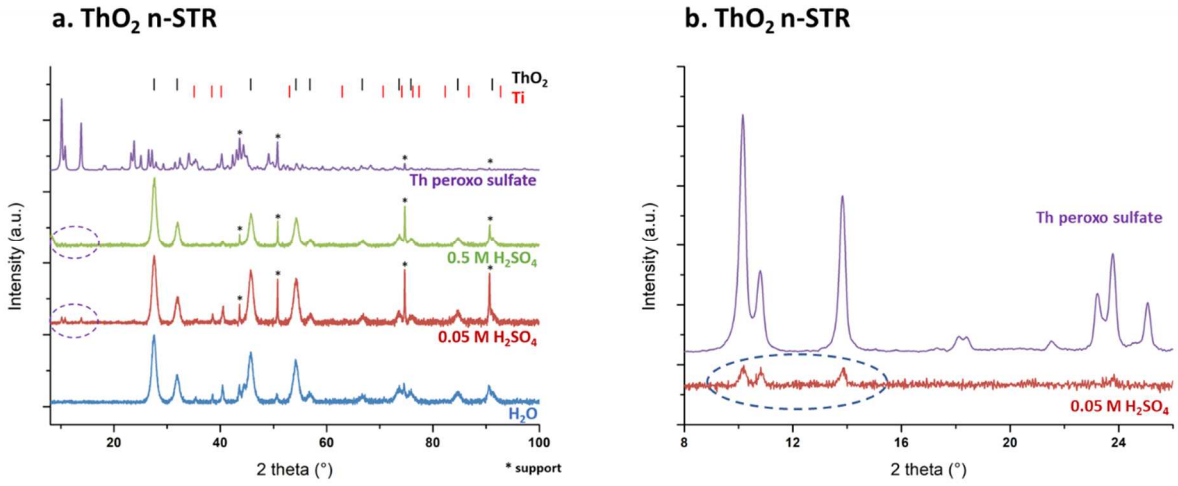

Figure 8: (a.) Normalized PXRD diagrams (background corrected) acquired on the sonolysis residues for nanostructured ThO_2 (485°C) treated in different media (20 kHz, Ar/(20%)O_2, 20°C, 0.34 W.mL^{-1}), and compared with the one of a thorium peroxo sulfate synthesized without ultrasound (purple spectrum).[56] Ticks stand for ICSD files for ThO_2 (ICSD 01-071-6407) and Ti (ICSD 00-044-1294). (b.) Magnification of the normalized PXRD diagram (background corrected) acquired on the sonolysis residue for nanostructured ThO_2 treated in 0.05 M H_2SO_4 (20 kHz, Ar/(20%)O_2, 20°C, 0.34 W.mL^{-1}), and compared with the one of a thorium peroxo sulfate synthesized without ultrasound.

Although high-frequency ultrasound generally enhance the sonochemical generation of H_2O_2 as expressed in **Figure 3** (see part 3.3.), the 345 kHz sonolysis of nanoscale ThO_2 in 0.05 M H_2SO_4 does not lead to the formation of Th peroxo sulfate species (**Figure S7, ESI**). This can be explained by the low dissolution of ThO_2 in these conditions (**Figure 2**, see part 3.2.) as a result of the absence of ThO_2 fragmentation and dispersion for such frequency. As it can be seen from PXRD data (**Figure S7, ESI**), a similar assessment can be mentioned in silent conditions, whatever the considered oxide. Although evidenced by PXRD (**Figure S4, ESI**), the formation of thorium peroxo sulfate during the sonication of ThO_2 nanopowder in 0.05 M sulfuric acid is not obvious with SEM observation. Sample residue indeed shows a padded morphology with ill-defined small grain aggregates (**Figure S8, ESI**). By contrast, SEM characterizations confirmed the formation of this new crystalline phase in the dissolution residue obtained after sonication of nanostructured ThO_2 (n-STR) in 0.05 M H_2SO_4 (**Figure 9**). A clear fragmentation and size reduction of the oxide platelets combined to the growth of a new phase forming fibers in agreement with the recently reported Th peroxo sulfate morphology [56], can be noted after 900 min of ultrasound. TEM experiments coupled with EDX spectroscopy consolidated the observation of the partial sonochemical conversion of ThO_2 into thorium peroxo sulfate. **Figure 10** shows a TEM image where a fiber particle is

observed close to small thorium oxide platelets. The EDX mapping confirmed the presence of thorium, oxygen and sulfur elements which support the formation of Th peroxo sulfate during the sonication of thorium oxide in sulfuric medium. The ThO_2 squared platelets also show thorium, oxygen and sulfur; the latter most probably resulting from the adsorption of sulfate on the surface of thorium oxide during sonolysis.

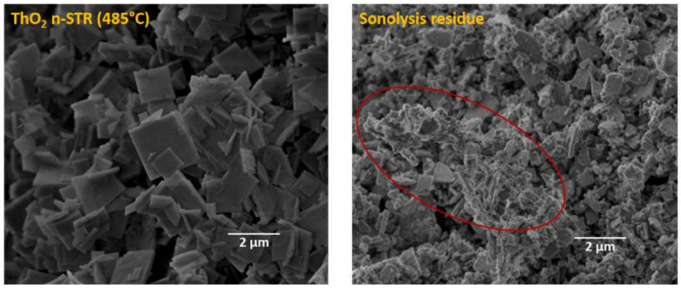

Figure 9: SEM images of nanostructured ThO_2 before (left) and after (right) sonication (20 kHz, Ar/(20%)O_2, 0.05 M H_2SO_4, 20°C, 0.34 W.mL^{-1}).

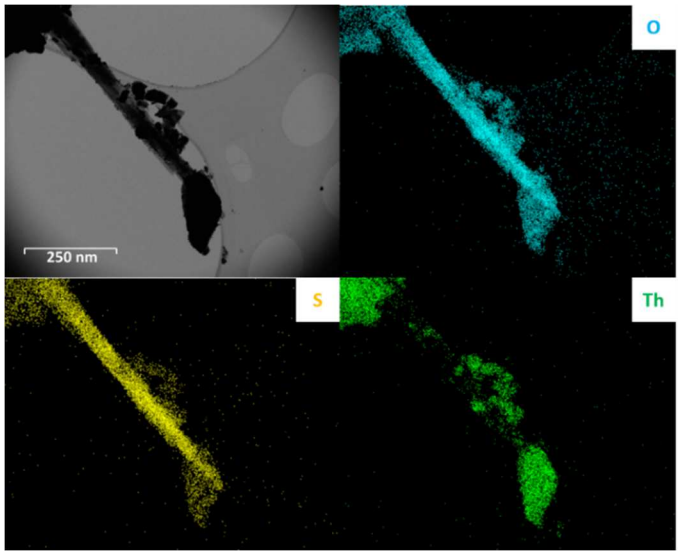

Figure 10: TEM images coupled with EDX mapping of the sonolysis residue obtained after 20 kHz sonication of nanostructured ThO_2 (485°C) in 0.05 M H_2SO_4 (Ar/(20%)O_2, 20°C, 0.34 W.mL^{-1}).

3.6. ThO_2 dissolution mechanism

The results described in the above discussion demonstrate that the significant dissolution of nanoscale ThO_2 samples observed in our conditions results from the physical (particle fragmentation and generation of defects) and chemical (generation of H_2O_2) effects driven by the 20 kHz acoustic cavitation phenomenon combined to an appropriate medium (sulfuric media in this case). The various results that arose this conclusion are summarized in **Table 2** to help in the proposition of a relevant dissolution mechanism for nanoscale ThO_2 samples.

Usually, the dissolution of thorium oxide described in the literature involves a surface mechanism with ion adsorption on the surface sites of the oxide, chemical complexation reaction between the solid surface and the adsorbed species and finally, desorption of the thorium complex [11,47]. The formation of thorium peroxo sulfate during the sonolysis of ThO_2 in sulfuric acid solution can be interpreted by two different processes: (i) a solution

coordination mechanism then precipitation, (ii) a surface complexation mechanism, or (iii) a combination of both processes.

Table 2: Summary of the different effects involved in ThO_2 n-STR dissolution.

Effect studied *(fixed conditions)*	**Parameters**	**$W_0(H_2O_2)$** ($\mu M.min^{-1}$)	**Dissolution yield** (%)	**Thorium peroxo sulfate** (x= yes)
Medium *(20 kHz; Ar/O_2)*	H_2O	0.7	0	-
	0.05 M H_2SO_4	3.2	3	X
	0.5 M H_2SO_4	1.6	20	X
Ultrasonic frequency *(0.05 M H_2SO_4; Ar/O_2)*	20 kHz	3.2	3	X
	345 kHz	20.5	1	-
	silent conditions	-	0.4	-
Atmosphere *(0.5 M H_2SO_4; 20 kHz)*	Ar/CO	-	6	-
	Ar	0.9	7	X
	Ar/O_2	1.6	20	X
Adding H_2O_2 *(0.05 M H_2SO_4; 20 kHz; Ar/O_2)*	-	3.2	3	X
	$[H_2O_2]$ = 0.01 M	-	11	X

In the former case, a dissolution/reprecipitation process would involve the presence of Th(IV) in solution that could then be complexed with sulfate and generated H_2O_2 in agreement with the previous report described elsewhere [56]. In this case, the low precipitation kinetics already observed for this compound combined with the low amount of species available in solution (e.g., H_2O_2 consumption occurs through dissolution and catalytic decomposition at ThO_2 surface, see part 3.3.) would explain the low conversion yields (kinetics and solubility product). The absence of Th peroxo sulfate at high ultrasonic frequency and at silent conditions (see part 3.5.) favors this mechanism, so as the observation of fibers having very different morphology if compared with initial ThO_2 (**Figure 9**, see part 3.5.).

Alternatively, H_2O_2 and sulfate ligands can form surface complexes and facilitate the dissolution of ThO_2 in the form of Th(IV) peroxo and/or sulfate complexes. According to **Table 2**, the sonochemical generation of H_2O_2 is mandatory for ThO_2 dissolution. Most probably, H_2O_2 adsorption can occur by the replacement of H_2O molecules at ThO_2 surface as it was reported recently (**Figure 11**).[57] The effect of H_2SO_4 concentration could be assigned to the protonation of ThO_2 surface (initial steps described by the equations Eq. 1-2, the symbol ")))" stands for 20 kHz ultrasound irradiation) although the adsorption of sulfate cannot be excluded in agreement with the literature.[58] The formation of a mixed surface complex could also be hypothesized. Nevertheless, the exact dissolution mechanism needs further investigations.

Surface hydrolysis and protonation:

$$\equiv ThO_2 + H_2O \rightarrow))) \rightarrow \equiv OTh(OH)_2 \quad (1)$$

$$\equiv OTh(OH)_2 + 2H^+ \rightarrow \equiv OTh(OH_2^+)_2 \quad (2)$$

Note that mixtures of concentrated H_2O_2 and H_2SO_4 solutions are used reactants for the preparation of Caro's acid (peroxymonosulfuric acid). The formation of such strong oxidant acid remains however highly unlikely in our conditions due to the low amount of involved reactants and the high instability of peroxymonosulfuric acid. Furthermore, sonolytic

decomposition or splitting of sulfuric species are unlikely in these conditions. Previous studies indeed demonstrated the possible degradation of sulfuric media at much higher concentrations (> 9 M) when non-dissociated H_2SO_4 molecules predominate in solution and are able to enter the cavitation bubble which is not the case in our study.[59–61] Speciation diagram provided in **Figure S9** (**ESI**) confirms that in our conditions (pH_{th}= 0.3 and 1.23 respectively in 0.5 and 0.05 M H_2SO_4), HSO_4^- is the predominant specie.

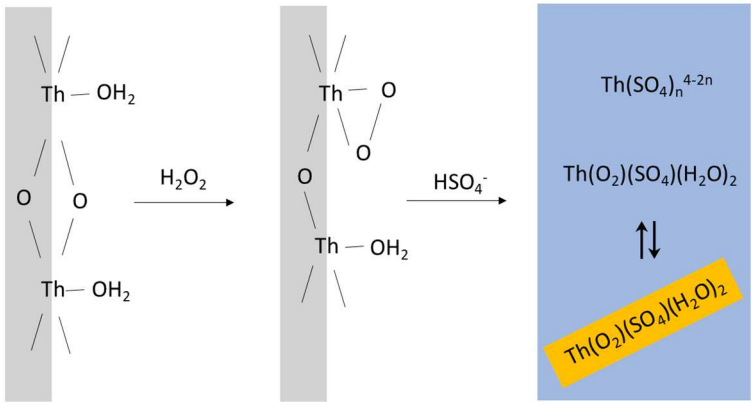

Figure 11: Scheme of the ultrasound-assisted dissolution of ThO_2.

4. Conclusion

This study confirms the enhanced reactivity of nanoscale thorium oxides under ultrasound irradiation. Although being highly refractive towards dissolution in silent conditions, the significant dissolution of ThO_2 can be achieved under 20 kHz sonication in dilute aqueous solutions of H_2SO_4. Dissolution rates and yields are strongly dependent upon (i) the physical effects driven by the acoustic cavitation such as the particle fragmentation or surface activation (strain, stress, hydrolysis, hydration, etc.), (ii) the sonochemical activity through the in-situ generation of hydrogen peroxide, and (iii) the complexing affinity of the medium (sulfate) towards the oxide surface. The highest dissolution yields are observed with ThO_2 nanopowder sonicated at 20 kHz under Ar/(20%)O_2 atmosphere in 0.5 M H_2SO_4. Characterizations of the sonolysis residues with PXRD, SEM and HR-TEM revealed the partial conversion of ThO_2 into a scarce Th peroxo sulfate complex, which can be explained by one or both of the following mechanisms: dissolution/reprecipitation process and/or formation of a surface activated complex. Further experiments are planned to clarify the dissolution mechanism and synthesize directly this compound under ultrasound with a thorium nitrate starting solution and with other counter-ions. In addition, the sonochemical reactivity of nanoscale PuO_2 in sulfuric acid solution will be studied while assuming the potential formation of an analogous Pu(IV) peroxo compound.

Acknowledgements

We acknowledge the financial support of RCHIM and PRATA research programs of CEA, the French Alternative Energies and Atomic Energy Commission. The authors are thankful to Adel Mesbah who performed the Rietveld refinements.

Reference

[1] M. Ichimiya, Y. Sagayama, A generation IV sodium-cooled fast reactor concept and its R&D program, Am. Nucl. Soc. 90 (2004) 46–47.

[2] W. Hoffelner, Materials for the Very High Temperature Reactor (VHTR): A versatile nuclear power station for combined cycle electricity and heat production, Chim. Int. J. Chem. 59 (2005) 977–982. https://doi.org/10.2533/000942905777675435.

[3] G. Heisbourg, S. Hubert, N. Dacheux, J. Ritt, The kinetics of dissolution of $Th_{1-x}U_xO_2$ solid solutions in nitric media, J. Nucl. Mater. 321 (2003) 141–151. https://doi.org/10.1016/S0022-3115(03)00213-7.

[4] L. Claparede, N. Clavier, N. Dacheux, A. Mesbah, J. Martinez, S. Szenknect, P. Moisy, Multiparametric dissolution of thorium–cerium dioxide solid solutions, Inorg. Chem. 50 (2011) 11702–11714. https://doi.org/10.1021/ic201699t.

[5] H.-D. Greiling, K.H. Lieser, Properties of ThO_2, UO_2 and PuO_2 as function of pretreatment and their dissolution in HNO_3, Radiochim. Acta. 35 (1984) 79–89.

[6] N. Desigan, N. Bhatt, M.A. Shetty, G.K.P. Sreekumar, N.K. Pandey, U. Kamachi Mudali, R. Natarajan, J.B. Joshi, Dissolution of nuclear materials in aqueous acid solutions, Rev. Chem. Eng. 35 (2019) 707–734. https://doi.org/10.1515/revce-2017-0063.

[7] M. Akabori, T. Shiratori, Dissolution of ThO_2 based oxides in nitric acid solutions at elevated temperatures, J. Nucl. Sci. Technol. 31 (1994) 539–545. https://doi.org/10.1080/18811248.1994.9735188.

[8] A.R. Keshtkar, S. Abbasizadeh, Activation energy determination and kinetic modeling of thorium oxide dissolution in nitric acid/ hydrofluoric acid system: Influence of fluoride ion on ThO_2 dissolution, Prog. Nucl. Energy. 93 (2016) 362–370. https://doi.org/10.1016/j.pnucene.2016.09.008.

[9] T. Takeuchi, C.K. Hanson, M.E. Wadsworth, Kinetics and mechanism of the dissolution of thorium oxide in hydrofluoric acid and nitric acid mixtures, J. Inorg. Nucl. Chem. 33 (1971) 1089–1098. https://doi.org/10.1016/0022-1902(71)80178-1.

[10] M. Simonnet, N. Barré, R. Drot, C.L. Naour, V. Sladkov, S. Delpech, Multiparametric study of thorium oxide dissolution in aqueous media, Radiochim. Acta. 104 (2016). https://doi.org/10.1515/ract-2016-2607.

[11] M. Simonnet, N. Barré, R. Drot, C. Le Naour, V. Sladkov, S. Delpech, Thorium oxide dissolution in HNO_3-HF mixture: kinetics and mechanism, Radiochim. Acta. 107 (2019) 289–297. https://doi.org/10.1515/ract-2018-3052.

[12] K. Lyczko, M. Lyczko, M. Walo, J. Lipkowski, Conversion of thorium(IV) oxide into thorium(IV) trifluoromethanesulfonate: Crystal structure of thorium(IV) trifluoromethanesulfonate dihydrate, Inorg. Chem. Commun. 24 (2012) 234–236. https://doi.org/10.1016/j.inoche.2012.07.024.

[13] N.N. Mirashi, S. Chaudhury, S.K. Aggarwal, Dissolution of sintered thorium dioxide in phosphoric acid using autoclave and microwave methods with detection by gamma spectrometry, Microchem. J. 94 (2010) 24–27. https://doi.org/10.1016/j.microc.2009.08.002.

[14] N. Sato, A. Kirishima, Sulfurization behavior of thorium dioxide with carbon disulfide, J. Nucl. Mater. 414 (2011) 324–327. https://doi.org/10.1016/j.jnucmat.2011.04.060.

[15] R.K. Malav, N.D. Save, A. Prakash, Md. Afzal, J.P. Panakkal, Use of indigenous microwave system for dissolution and treatment of waste from nuclear materials, J. Radioanal. Nucl. Chem. 295 (2013) 425–430. https://doi.org/10.1007/s10967-012-1790-2.

[16] H. Gleiter, Nanostructured materials: Basic concepts and microstructure, Acta Mater. 48 (2000) 1–29.

[17] M. Fernández-García, A. Martínez-Arias, J.C. Hanson, J.A. Rodriguez, Nanostructured oxides in chemistry: Characterization and properties, Chem. Rev. 104 (2004) 4063–4104. https://doi.org/10.1021/cr030032f.

[18] J.-M. Teulon, C. Godon, L. Chantalat, C. Moriscot, J. Cambedouzou, M. Odorico, J. Ravaux, R. Podor, A. Gerdil, A. Habert, N. Herlin-Boime, S. Chen, J.-L. Pellequer, On the operational aspects of measuring nanoparticle sizes, Nanomaterials. 9 (2018) 18. https://doi.org/10.3390/nano9010018.

[19] W.J. Stark, P.R. Stoessel, W. Wohlleben, A. Hafner, Industrial applications of nanoparticles, Chem. Soc. Rev. 44 (2015) 5793–5805. https://doi.org/10.1039/C4CS00362D.

[20] G. Heisbourg, S. Hubert, N. Dacheux, J. Purans, Kinetic and thermodynamic studies of the dissolution of thoria-urania solid solutions, J. Nucl. Mater. 335 (2004) 5–13. https://doi.org/10.1016/j.jnucmat.2004.05.017.

[21] S. Hubert, K. Barthelet, B. Fourest, G. Lagarde, N. Dacheux, N. Baglan, Influence of the precursor and the calcination temperature on the dissolution of thorium dioxide, J. Nucl. Mater. (2001) 8.

[22] E. Myllykylä, T. Lavonen, M. Stennett, C. Corkhill, K. Ollila, N. Hyatt, Solution composition and particle size effects on the dissolution and solubility of a ThO_2 microstructural analogue for UO_2 matrix of nuclear fuel, Radiochim. Acta. 103 (2015). https://doi.org/10.1515/ract-2014-2271.

[23] R.D. Shannon, Revised effective ionic radii and systematic studies of interatomic distances in halides and chalcogenides, Acta Crystallogr. Sect. A. 32 (1976) 751–767. https://doi.org/10.1107/S0567739476001551.

[24] S.I. Nikitenko, L. Venault, R. Pflieger, T. Chave, I. Bisel, P. Moisy, Potential applications of sonochemistry in spent nuclear fuel reprocessing: A short review, Ultrason. Sonochem. 17 (2010) 1033–1040. https://doi.org/10.1016/j.ultsonch.2009.11.012.

[25] F. Juillet, J.M. Adnet, M. Gasgnier, Ultrasound effects on the dissolution of refractory oxides (CeO_2 and PuO_2) in nitric acid, J. Radioanal. Nucl. Chem. 224 (1997) 137–143. https://doi.org/10.1007/BF02034626.

[26] Ph. Moisy, S.I. Nikitenko, L. Venault, C. Madic, Sonochemical dissolution of metallic plutonium in a mixture of nitric and formic acid, Radiochim. Acta. 75 (1996). https://doi.org/10.1524/ract.1996.75.4.219.

[27] M. Virot, S. Szenknect, T. Chave, N. Dacheux, P. Moisy, S.I. Nikitenko, Uranium carbide dissolution in nitric solution: Sonication vs. silent conditions, J. Nucl. Mater. 441 (2013) 421–430. https://doi.org/10.1016/j.jnucmat.2013.06.021.

[28] M. Virot, L. Venault, P. Moisy, S.I. Nikitenko, Sonochemical redox reactions of Pu(III) and Pu(IV) in aqueous nitric solutions, Dalton Trans. 44 (2015) 2567–2574. https://doi.org/10.1039/C4DT02330G.

[29] X. Beaudoux, M. Virot, T. Chave, G. Leturcq, G. Jouan, L. Venault, P. Moisy, S.I. Nikitenko, Ultrasound-assisted reductive dissolution of CeO_2 and PuO_2 in the presence of Ti particles, Dalton Trans. 45 (2016) 8802–8815. https://doi.org/10.1039/C5DT04931H.

[30] E. Dalodière, M. Virot, V. Morosini, T. Chave, T. Dumas, C. Hennig, T. Wiss, O. Dieste Blanco, D.K. Shuh, T. Tyliszcak, L. Venault, P. Moisy, S.I. Nikitenko, Insights into the sonochemical synthesis and properties of salt-free intrinsic plutonium colloids, Sci. Rep. 7 (2017). https://doi.org/10.1038/srep43514.

[31] H. Bouyarmane, A. Gouza, S. Masse, S. Saoiabi, A. Saoiabi, T. Coradin, A. Laghzizil, Nanoscale conversion of chlorapatite into hydroxyapatite using ultrasound irradiation,

Colloids Surf. Physicochem. Eng. Asp. 495 (2016) 187–192. https://doi.org/10.1016/j.colsurfa.2016.02.014.
[32] K. Prasad, D.V. Pinjari, A.B. Pandit, S.T. Mhaske, Phase transformation of nanostructured titanium dioxide from anatase-to-rutile via combined ultrasound assisted sol–gel technique, Ultrason. Sonochem. 17 (2010) 409–415. https://doi.org/10.1016/j.ultsonch.2009.09.003.
[33] S. Hubert, G. Heisbourg, N. Dacheux, P. Moisy, Effect of inorganic ligands and hydrogen peroxide on ThO_2 dissolution. Behaviour of $Th_{0.87}Pu_{0.13}O_2$ during leaching test, Inorg. Chem. 47 (2008) 2064–2073. https://doi.org/10.1021/ic702065z.
[34] X. Beaudoux, M. Virot, T. Chave, G. Durand, G. Leturcq, S.I. Nikitenko, Vitamin C boosts ceria-based catalyst recycling, Green Chem. 18 (2016) 3656–3668. https://doi.org/10.1039/C6GC00434B.
[35] V. Morosini, T. Chave, M. Virot, P. Moisy, S.I. Nikitenko, Sonochemical water splitting in the presence of powdered metal oxides, Ultrason. Sonochem. 29 (2016) 512–516. https://doi.org/10.1016/j.ultsonch.2015.11.006.
[36] L. Bonato, M. Virot, T. Dumas, A. Mesbah, E. Dalodière, O. Dieste, T. Wiss, X.F. Le Goff, M. Odorico, D. Prieur, A. Rossberg, L. Venault, N. Dacheux, P. Moisy, S. Nikitenko, Probing the local structure of nanoscaled actinide oxides: A comparison between PuO_2 and ThO_2 nanoparticles rules out PuO_{2+x} hypothesis, Nanoscale Adv. (2019). https://doi.org/10.1039/C9NA00662A.
[37] S.I. Nikitenko, C. Le Naour, P. Moisy, Comparative study of sonochemical reactors with different geometry using thermal and chemical probes, Ultrason. Sonochem. 14 (2007) 330–336. https://doi.org/10.1016/j.ultsonch.2006.06.006.
[38] S.I. Nikitenko, P. Martinez, T. Chave, I. Billy, Sonochemical disproportionation of carbon monoxide in water: Evidence for treanor effect during multibubble cavitation, Angew. Chem. Int. Ed. 48 (2009) 9529–9532. https://doi.org/10.1002/anie.200904275.
[39] C. Frontera, J. Rodriguez-Carvajal, Phys. B Condens. Matter. 335 (2003) 219–222.
[40] C. Petrier, A. Jeunet, J.L. Luche, G. Reverdy, Unexpected frequency effects on the rate of oxidative processes induced by ultrasound, J. Am. Chem. Soc. 114 (1992) 3148–3150. https://doi.org/10.1021/ja00034a077.
[41] M.A. Beckett, I. Hua, Impact of ultrasonic frequency on aqueous sonoluminescence and sonochemistry, J. Phys. Chem. A. 105 (2001) 3796–3802. https://doi.org/10.1021/jp003226x.
[42] E. Dalodière, M. Virot, P. Moisy, S.I. Nikitenko, Effect of ultrasonic frequency on H_2O_2 sonochemical formation rate in aqueous nitric acid solutions in the presence of oxygen, Ultrason. Sonochem. 29 (2016) 198–204. https://doi.org/10.1016/j.ultsonch.2015.09.014.
[43] R. Pflieger, T. Chave, G. Vite, L. Jouve, S.I. Nikitenko, Effect of operational conditions on sonoluminescence and kinetics of H_2O_2 formation during the sonolysis of water in the presence of Ar/O_2 gas mixture, Ultrason. Sonochem. 26 (2015) 169–175. https://doi.org/10.1016/j.ultsonch.2015.02.005.
[44] V. Raman, G.V. Jere, Physico-chemical studies on thorium peroxosulphate, Indian J. Chem. 11 (1973) 31–34.
[45] C.R. Bhattacharjee, M.K. Chaudhuri, R.N. Dutta Purkayastha, New heteroligand peroxothorates(IV) of the type $A_2[Th(O_2)F_2(OH)_2].nH_2O$ (A = NH_4, n = 3; A = Na or K, n = 1) and molecular peroxothorium(IV) complexes of the type $[Th_2(O_2)_3L(H_2O)_4].5H_2O$ (L = C_2O_4 or SO_4), Inorganica Chim. Acta. 160 (1989) 147–152.
[46] C.R. Bhattacharjee, Peroxothorium(IV) complexes containing hydroxo and phosphato coligands. Spectroscopic evidence for η2 and σ:σ peroxide, J. Coord. Chem. 34 (1995) 215–220.

[47] L. Claparede, F. Tocino, S. Szenknect, A. Mesbah, N. Clavier, P. Moisy, N. Dacheux, Dissolution of $Th_{1-x}U_xO_2$: Effects of chemical composition and microstructure, J. Nucl. Mater. 457 (2015) 304–316. https://doi.org/10.1016/j.jnucmat.2014.11.094.

[48] G.R. Patzke, Y. Zhou, R. Kontic, F. Conrad, Oxide nanomaterials: Synthetic developments, mechanistic studies, and technological innovations, Angew. Chem. Int. Ed. 50 (2011) 826–859. https://doi.org/10.1002/anie.201000235.

[49] V. Tyrpekl, J.-F. Vigier, D. Manara, T. Wiss, O. Dieste Blanco, J. Somers, Low temperature decomposition of U(IV) and Th(IV) oxalates to nanograined oxide powders, J. Nucl. Mater. 460 (2015) 200–208. https://doi.org/10.1016/j.jnucmat.2015.02.027.

[50] K. Popa, O. Walter, O.D. Blanco, A. Guiot, D. Bouëxière, J.-Y. Colle, L. Martel, M. Naji, D. Manara, A low-temperature synthesis method for AnO_2 nanocrystals (An = Th, U, Np, and Pu) and associate solid solutions, CrystEngComm. 20 (2018) 4614–4622. https://doi.org/10.1039/C8CE00446C.

[51] A.K. Arora, M. Rajalakshmi, T.R. Ravindran, V. Sivasubramanian, Raman spectroscopy of optical phonon confinement in nanostructured materials, J. Raman Spectrosc. 38 (2007) 604–617. https://doi.org/10.1002/jrs.1684.

[52] K. Kamali, K. Ananthasivan, T.R. Ravindran, D.S. Kumar, High pressure Raman spectroscopic studies on nanocrystalline ThO_2, J. Nucl. Mater. 493 (2017) 77–83. https://doi.org/10.1016/j.jnucmat.2017.05.048.

[53] F. Cappia, D. Hudry, E. Courtois, A. Janßen, L. Luzzi, R.J.M. Konings, D. Manara, High-temperature and melting behaviour of nanocrystalline refractory compounds: an experimental approach applied to thorium dioxide, Mater. Res. Express. 1 (2014) 025034. https://doi.org/10.1088/2053-1591/1/2/025034.

[54] N. Aničić, M. Vukomanović, T. Koklič, D. Suvorov, Fewer defects in the surface slows the hydrolysis rate, decreases the ROS generation potential, and improves the non-ROS antimicrobial activity of MgO, Small. 14 (2018) 1800205. https://doi.org/10.1002/smll.201800205.

[55] M. Vasiliu, K.A. Peterson, J.K. Gibson, D.A. Dixon, Reliable potential energy surfaces for the reactions of H_2O with ThO_2 , PaO_2^+, UO_2^{2+}, and UO_2^+, J. Phys. Chem. A. 119 (2015) 11422–11431. https://doi.org/10.1021/acs.jpca.5b08618.

[56] L. Bonato, M. Virot, T. Dumas, A. Mesbah, P. Lecante, D. Prieur, X. Le Goff, C. Hennig, N. Dacheux, P. Moisy, S.I. Nikitenko, Deciphering the crystal structure of a scarce 1D polymeric thorium peroxo sulfate, Chem. – Eur. J. 25 (2019) 9580–9585. https://doi.org/10.1002/chem.201901426.

[57] C.M. Lousada, A.J. Johansson, T. Brinck, M. Jonsson, Mechanism of H_2O_2 decomposition on transition metal oxide surfaces, J. Phys. Chem. C. 116 (2012) 9533–9543.

[58] N. Kitadai, K. Nishiuchi, M. Tanaka, A comprehensive predictive model for sulfate adsorption on oxide minerals, Geochim. Cosmochim. Acta. 238 (2018) 150–168.

[59] G.L. Sharipov, A.M. Abdrakhmanov, R.Kh. Gainetdinov, Sonoluminescence of aqueous solutions of sulfuric acid and sulfur dioxide, Russ. Chem. Bull. 52 (2003) 1966–1968.

[60] M.V. Nikonov, V.P. Shilov, The destruction of sulfuric acid induced by ultrasonic vibrations, Russ. Chem. Bull. 43 (1994) 1087.

[61] A. Moshaii, Kh. Imani, M. Silatani, Sonoluminescence radiation from different concentrations of sulfuric acid, Phys. Rev. E. 80 (2009) 046325.